

**Orbital angular momentum structure of an unoccupied spin-split quantum-well state in Pb/Cu(111)**S. Jakobs,<sup>1,2,\*</sup> A. Ruffing,<sup>1</sup> M. Cinchetti,<sup>1</sup> S. Mathias,<sup>1</sup> and M. Aeschlimann<sup>1</sup><sup>1</sup>*Department of Physics and Research Center OPTIMAS, University of Kaiserslautern, 67663 Kaiserslautern, Germany*<sup>2</sup>*Graduate School Materials Science in Mainz, Erwin Schroedinger Straße 46, 67663 Kaiserslautern, Germany*

(Received 19 April 2013; published 28 June 2013)

We performed circular dichroism angle-resolved two-photon photoemission experiments on the quantum-well system one monolayer Pb on Cu(111) to investigate the orbital angular momentum (OAM) structure of the unoccupied quantum-well state. The Pb/Cu(111) system exhibits a small Rashba-type spin-orbit splitting of the unoccupied band around the  $\bar{\Gamma}$  point and can be referred to as a material system with an intermediate spin-orbit coupling (SOC) parameter. As predicted by Kim *et al.* [*Phys. Rev. B* **85**, 195402 (2012)], systems with such intermediate SOC strength should show a reversal of the OAM direction for the inner band of a spin-split system. Our results show dichroism values up to  $\pm 20\%$  and also the expected change of the dichroism signal at a finite  $k_{\parallel}$  point. The circular dichroism angle-resolved photoemission results therefore support the sensitivity of circular dichroism to OAM texture additionally to spin texture, and also that local OAM must be included to describe the experimentally observed large spin splittings in Rashba systems.

DOI: [10.1103/PhysRevB.87.235438](https://doi.org/10.1103/PhysRevB.87.235438)

PACS number(s): 73.20.-r, 79.60.-i, 73.21.Fg

**I. INTRODUCTION**

The Rashba-Bychkov effect can explain the lifting of degenerate bands in the electronic band structure of a solid due to the breaking of the space inversion symmetry at, for instance, interfaces or surfaces.<sup>1</sup> Various observed spin textures in spin-split surface states and quantum-well states were successfully explained by this Rashba model.<sup>2-5</sup> However, it could not reveal the appropriate magnitude of the energetic splitting, which is explained in the Rashba model by the combination of a large spin-orbit coupling and a relativistic Zeeman splitting.<sup>1</sup> Experimentally observed Rashba-type spin-orbit split systems show energetic splittings in the meV range, which is  $10^5$  times larger than theoretically predicted by the standard Rashba effect.<sup>6</sup> It has been shown that an in-plane potential gradient, e.g., for the surface alloys Bi/Ag(111) and Sb/Ag(111), can induce such large spin splittings.<sup>7,8</sup> This gives rise to out-of-plane spin polarization components<sup>7</sup> and also unconventional spin textures with parallel aligned spins, which originate from the hybridization of surface states with different orbital characters.<sup>9</sup> Furthermore, the interaction of atomic and structural contributions also have to be taken into account.<sup>10</sup>

In recent publications another alternative model that overcomes the discrepancies of the pure Rashba model with respect to the energetic splitting was introduced.<sup>6,11,12</sup> It was shown that the existence of local orbital angular momentum (OAM) is responsible for the large observed splittings in a Rashba-type spin-orbit split system. In this description, an electric dipole is induced by a local OAM state in the Bloch wave functions.<sup>11</sup> As a consequence of the broken inversion symmetry at the surface of a crystal, an electric field perpendicular to the surface aligns the electric dipole and leads to the forming of chiral OAM states and the characteristic splitting. This new approach including local OAM for the explanation of Rashba-type band splitting is still under heavy discussion,<sup>13,14</sup> and therefore further measurements showing the sensitivity of circular dichroism to OAM are helpful. Kim *et al.* furthermore developed an effective Hamiltonian to investigate the behavior of OAM and spin as a function

of the atomic spin-orbit coupling (SOC) parameter  $\alpha$ .<sup>6</sup> As a spin and OAM sensitive method, they used circular dichroism photoemission spectroscopy to investigate the OAM structure in various systems. With their model, they were able to explain the dichroic signal for the surface states of Cu(111) and Au(111) (small SOC parameter  $\alpha$ ) and for Bi<sub>2</sub>Se<sub>3</sub> (large SOC parameter  $\alpha$ ).<sup>6,15</sup> For the intermediate case they made the prediction that the OAM *reverses* at a finite momentum for the inner band of a Rashba-type spin-orbit split system. However, they were not able to address this intermediate case experimentally, so far. Hence it would be interesting to find suitable systems that show the transition from the small to the intermediate case for the evolution of OAM as a function of  $\alpha$ , which we now present in this paper. We use circular dichroism in angle-resolved photoemission spectroscopy (CD-ARPES) to study the unoccupied spin-split quantum-well states (QWS) of Pb/Cu(111) using two-photon photoemission (2PPE). We find the predicted OAM reversal at finite momentum, and therewith support the idea of the sensitivity of CD-ARPES to local OAM in addition to spin.<sup>16</sup>

**II. EXPERIMENTAL SETUP**

The ARPES measurements were performed using a hemispherical two-dimensional electron analyzer under ultrahigh vacuum conditions with a base pressure in the low  $10^{-10}$  mbar range. We set the pass energy at 20 eV resulting in an energetic resolution of 20 meV and an angular resolution of  $0.3^\circ$ . The Cu(111) single crystal is cleaned by argon ion sputtering and annealing cycles and the surface quality is checked by low energy electron diffraction (LEED) and the linewidth of the Shockley surface state. The ultrathin metal films are deposited with an effusion cell. The preparation procedure is as follows: First, more than 1 ML (monolayer) of Pb is grown on the clean Cu(111) crystal. In the second step, the film is annealed to 600 K to remove spare atoms, and a coverage of only 1 ML is left. The quality of the film is checked by LEED. The LEED pattern of the Pb film shows a clear  $4 \times 4$  structure (not shown here).<sup>17,18</sup> A more detailed preparation procedure

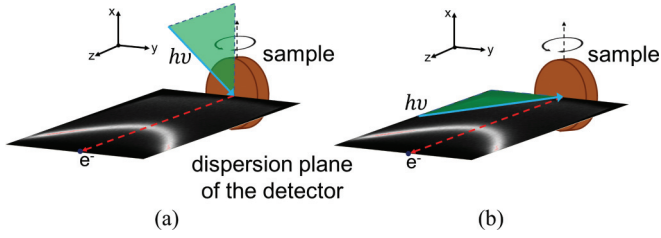


FIG. 1. (Color online) Schematic view of the experimental geometry. The experiments were performed in two different excitation directions: In both geometries the incidence angle of the laser light is  $45^\circ$  to the normal of the sample. In (a) the incoming laser light is in the perpendicular plane ( $x$ - $z$  plane) to the detector's dispersion plane ( $y$ - $z$  plane) in contrast to the setup used in (b). Here, the incoming direction of the circularly polarized photons is within in the  $y$ - $z$  plane. These two geometries allow one to probe all three directions  $x$ ,  $y$ , and  $z$  of a possible OAM component.

is provided in Ref. 19. During the photoemission experiments, the sample was held at room temperature. A bias voltage of  $U = -5$  V between sample and analyzer was applied. As a light source we used the second harmonic ( $h\nu = 2.95$  eV) of a mode-locked narrow-bandwidth Ti:sapphire laser system (bandwidth  $\approx 20$  meV, repetition rate 80 MHz, pulse duration 100 fs) that delivers linearly polarized pulses. The circularity of the photons is changed by a  $\lambda/4$  plate mounted on a computer assisted rotation stage that automatically changes the polarization from  $\sigma^-$  to  $\sigma^+$ . The difference of the measured spectra for left  $\sigma^-$  and right  $\sigma^+$  circularly polarized light divided by the sum defines the normalized circular dichroism (NCD):

$$\text{NCD} = \frac{I_{\sigma^+} - I_{\sigma^-}}{I_{\sigma^+} + I_{\sigma^-}}. \quad (1)$$

The used experimental setup is shown in Figs. 1(a) and 1(b): In (a) the direction of the incoming laser beam is in the perpendicular plane to the dispersion plane of our detector and hits the sample under an angle of  $45^\circ$  relative to the surface normal. In (b) the direction of the incoming laser beam lies in the dispersion plane of our detector. Setup (a) is sensitive to the in-plane spin and OAM component for circular dichroism measurements, and (b) is sensitive to the out-of-plane components. As is the case for OAM, as well as for the alignment of the spins in Rashba systems, the predominant direction lies in the surface and points perpendicular to the parallel momentum  $\vec{k}_\parallel$  of the (photo)electrons<sup>3,6,11,12,20</sup> [in-plane spin and OAM components, measured with geometry (a)]. Nevertheless, we need the second geometrical setup shown in Fig. 1(b) to prove later that no out-of-plane components might induce the below described experimental observations.

### III. RESULTS AND DISCUSSION

#### A. Orbital angular momentum as a function of spin-orbit coupling

We first want to discuss the expected OAM structure for systems with different SOC strength, as was predicted by Kim *et al.*<sup>6</sup> They were able to calculate the evolution of spin and OAM structures for spin-split inner and outer bands as a function of atomic SOC parameter  $\alpha$  [see Fig. 2(b)]

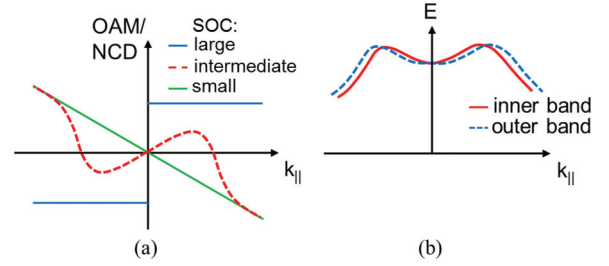


FIG. 2. (Color online) (a) Schematic behavior of projection of the OAM vector as a function of  $k_\parallel$  for different SOC strengths for the inner band adapted from Kim *et al.*<sup>6</sup> The direction of OAM for the outer band behaves the same for all SOC parameters and can be compared with the small SOC case of the inner band. (b) Schematic view of the Rashba-type spin-orbit split-band structure of the unoccupied QWS Pb/Cu(111) [see experimental results in Fig. 4] to distinguish between inner and outer bands.

for definition of the inner and outer bands, in particular, for the later discussed QWS Pb/Cu(111)]. They found a chiral behavior of both spin and OAM with a nearly linear  $k_\parallel$  dependence of OAM for small and intermediate SOC strengths.

Classifying the SOC dependence in a small, intermediate and strong case, they did show that the OAM vector of the outer band is antiparallel to the spin for all cases. For the inner band, however, they found a strong dependence of the OAM on the SOC strength. For systems with small SOC values, showing a degenerate band structure or only small splitting, the OAM of the inner and outer bands behaves identically and forms a chiral structure with a *parallel* alignment. The large SOC case exhibits a large splitting of the bands due to an *antiparallel* alignment of OAM for the inner and outer bands. These two cases could be experimentally confirmed with circular dichroism measurements on the surface states of Cu(111) and Au(111) (small SOC) and the topologically induced surface state of Bi<sub>2</sub>Se<sub>3</sub>.<sup>6,15</sup> Note, in particular, that these measurements also indicate that circular dichroism photoemission can be predominantly sensitive to the OAM texture, and not only to spin.<sup>16</sup>

Furthermore, Kim *et al.* make a very interesting prediction of the OAM alignment for intermediate SOC strengths.<sup>6</sup> Here, the inner band exhibits a transition pointing antiparallel to the spin of the inner band and to the OAM vector of the outer band near the  $\bar{\Gamma}$  point with a reverse of its direction at a finite  $k_\parallel$  point. This means that for small  $k_\parallel$  values the OAM structure is comparable to the large SOC case, and for large  $k_\parallel$  values it shows the same structure as for small SOC parameters. This behavior can be attributed to the fact that the atomic spin-orbit coupling  $\hat{H}_{\text{SOC}}$  is stronger for small  $k_\parallel$  values compared to the surface electric field  $\hat{H}_{\text{ES}}$ . Therefore, the OAM vector stays antiparallel to the spin. For larger  $k_\parallel$  values,  $\hat{H}_{\text{ES}}$  becomes larger than  $\hat{H}_{\text{SOC}}$  and the system will lower its energy by a parallel alignment of spin and OAM vectors.<sup>6,11</sup> Note that this reversal of the OAM for the inner band could not be experimentally confirmed so far, but would present another confirmation that OAM is important for a full description of Rashba systems.

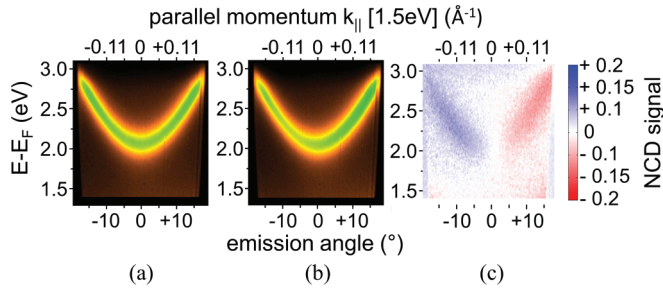


FIG. 3. (Color online) ARPES results for the surface state of Cu(111) for right (a) and left (b) circularly polarized photons. The spectra were taken using geometry Fig. 1(a). (c) NCD spectra.

Figure 2 summarizes the above described behavior of the OAM and the corresponding NCD signal for the inner band for small (green), intermediate (red dashed), and large (blue) SOC, as expected in our experimental geometry [cf. Fig. 1(a)]. Note that the direction of the OAM for the outer band for all SOC strengths behaves like the green line in Fig. 2(a). For small SOC, the inner band shows positive OAM for negative  $k_{\parallel}$ , and negative OAM for positive  $k_{\parallel}$ . For large SOC, the behavior of the inner band is vice versa, but without the linear  $k_{\parallel}$  dependence, and for intermediate SOC, there is an additional flip of OAM at finite momentum. Figure 2(b) illustrates the notation of the outer and inner bands, in particular, with respect to the here investigated QWS of the Pb/Cu system, where the free-electron-like parabola of the QWS shows an additional downward dispersing sidearm at higher momentum  $k_{\parallel}$ .

Now we want to present measurements on the surface state of Cu(111), a material with comparably small SOC. Additionally we want to show that CD-ARPES works in combination with 2PPE. Figure 3 shows the results of a CD-ARPES measurement on the surface state of Cu(111). In Fig. 3(a) [Fig. 3(b)] the spectra for right (left) circularly polarized photons are shown. The resulting dichroism spectra can be seen in Fig. 3(c). The surface state shows a clear difference in the sign of the NCD signal between negative and positive  $k_{\parallel}$  values. This behavior can now be directly compared with Fig. 2(a), and corresponds, as expected, to the green solid line. For small SOC parameters, the OAM is positive for negative  $k_{\parallel}$  values and vice versa.<sup>21</sup> This was already shown by Kim *et al.*, where they measured CD-ARPES of the surface states of Cu(111) and Au(111).<sup>6</sup> The behavior and also the magnitude of the circular dichroism values are comparable to our results for the surface state of Cu(111). The here repeated CD-ARPES experiment on Cu(111), now using 2PPE, confirms that the relevant circular dichroism signal is conserved under a two-photon excitation.

### B. Pb/Cu(111) as a material system with intermediate spin-orbit coupling

In the following, we will present our experimental results of CD-ARPES 2PPE measurements on the unoccupied QWS of 1 ML Pb/Cu(111), which can be referred to as the intermediate SOC case. First, we want to distinguish between inner and outer band contributions to the NCD signal. Afterwards, we

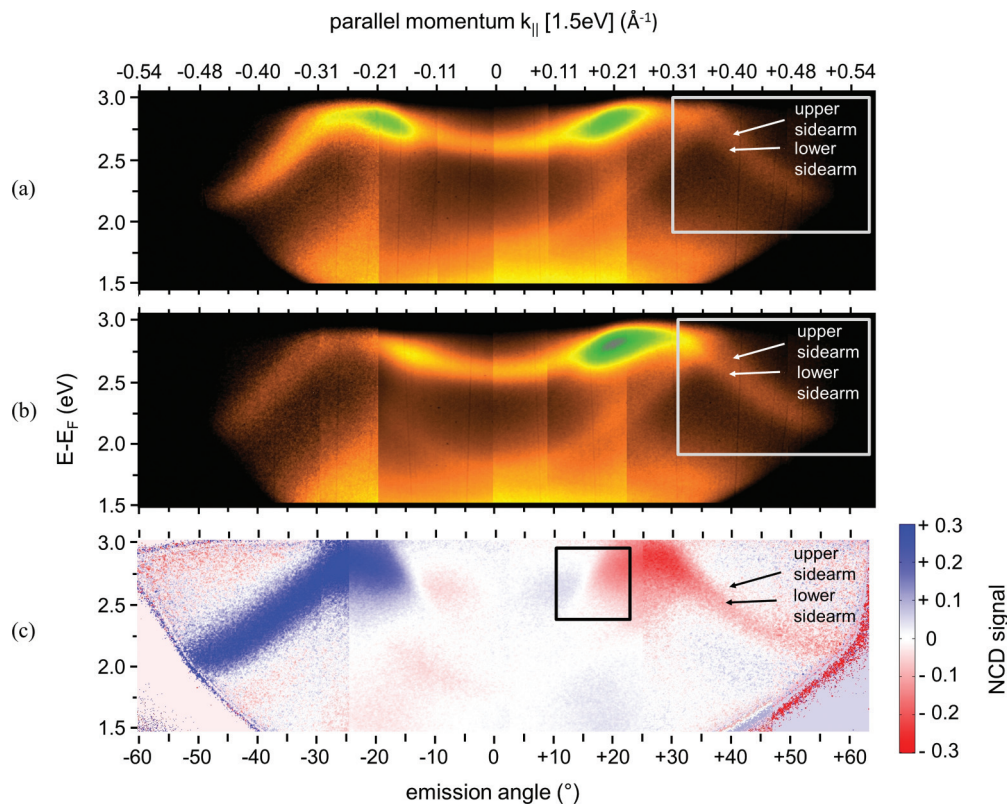


FIG. 4. (Color online) Experimental results of CD-2PPE-ARPES on Pb/Cu(111) for right (a) and left (b) circularly polarized photons and the resulting NCD spectra (c). The spectra were taken with the experimental geometry shown in Fig. 1(a) (Ref. 22).

will focus on the specific behavior of the NCD signal of the inner band.

### 1. Inner and outer band contribution to the NCD signal

Performing 2PPE with circularly polarized light, we investigate the unoccupied region of 1 ML Pb/Cu(111). In Fig. 4 the 2PPE spectra of Pb/Cu(111) for right [Fig. 4(a)] and left [Fig. 4(b)] circularly polarized photons are shown. The resulting normalized difference spectra can be seen in Fig. 4(c). The spectra show an unoccupied quantum-well state with the parabolic band bottom at the  $\bar{\Gamma}$  point at an energy of  $E - E_F = 2.65$  eV. Additionally to this free-electron-like parabolic behavior around the  $\bar{\Gamma}$  point, this particular QWS shows a downward dispersing sidearm at higher  $k_{\parallel}$  momentum [cf. Fig. 2(b) and Ref. 19]. Note that the Rashba-type spin-orbit splitting cannot be identified around the  $\bar{\Gamma}$  point due to the limited energy resolution and the flat dispersion of the quantum-well band. The splitting can be seen, however, at higher emission angles [see Figs. 4 (gray rectangle) and 2(b)], where a small splitting in a lower and upper downward dispersing sidearm is visible. Focusing on the NCD values of the sidearms [see Fig. 4(c)], one can see that while the lower sidearm shows a clear dichroism signal, the dichroism signal for the upper sidearm is completely quenched. This observation can be expected to be caused by differing contributions to the OAM from  $p$  and  $d$  orbitals, as was previously shown for the surface state of Au(111).<sup>6</sup> There, Kim *et al.* also found that the inner band of the Rashba-type spin-orbit split surface state shows much larger dichroism in comparison to the outer band. They explained this observation as a result of atomic orbital dependent contributions to OAM, which are different for the two bands. For the Pb/Cu(111) system, the lower sidearm indeed belongs to the so-called inner band, in agreement with the observation of Kim *et al.* [compare with Fig. 2(b)]. Considering the overall small total dispersion, it seems reasonable to assume that the same orbital contributes to the electronlike parabolic part and the downward dispersing sidearm of the state. In order to fully confirm these conclusions, DFT calculations need to be done to obtain the different orbital contributions to the OAM and therefore to the circular dichroism signal. Nevertheless, we conclude here that the experimentally observed lack of NCD signal from the upper arm (outer band) is sufficient indication that we see in our measurements predominantly the NCD signal of the inner band.

### 2. Orbital angular momentum reversal of the inner band

Let us now have a closer look at the behavior of the NCD signal of the inner quantum-well band around the  $\bar{\Gamma}$  point. As was also observed in the dichroism data of the surface states of Cu(111) and Au(111) by Kim *et al.*<sup>6</sup> and illustrated in Fig. 2(a), the NCD values increase with increasing momentum  $k_{\parallel}$ . However, in our results the dichroism signal of the quantum-well band vanishes at finite momentum  $k_{\parallel}$  and then changes its sign [see black square in Fig. 4(c)] from positive to negative values (or vice versa depending on positive or negative emission angles). To investigate this behavior in detail, we take the NCD values of the quantum-well band at different emission angles [see Fig. 5, lower spectrum in

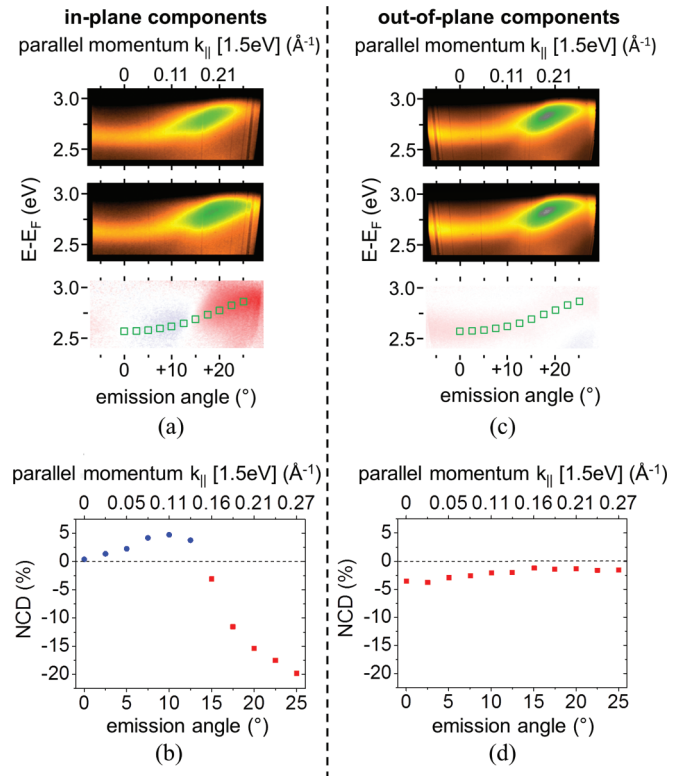


FIG. 5. (Color online) CD-2PPE spectra of Pb/Cu(111) taken at an emission angle of  $+10^\circ$  using two different geometries. (a) CD-2PPE spectra for right (up) and left (middle) circularly polarized light and the resulting normalized difference spectra (bottom) taken with the in-plane sensitive geometry shown in Fig. 1(a). (b) NCD values as a function of parallel momentum  $k_{\parallel}$  in the quantum-well band. The areas from which the dichroism values were taken are highlighted by green squares in the dichroism spectrum. (c) Same spectra as in (a), but taken with the out-of-plane sensitive geometry shown in Fig. 1(b). (d) From (c) extracted circular dichroism values as a function of parallel momentum  $k_{\parallel}$  in the quantum-well band.

(a)] and plot these NCD values as a function of the emission angle respectively parallel momentum  $k_{\parallel}$  [see Fig. 5(b)]. One can see the expected proportional dependence of the signal to the parallel momentum  $k_{\parallel}$ , where the NCD values increase from 0% at the  $\bar{\Gamma}$  point to  $+4.7\%$  at  $k_{\parallel} = 0.11 \text{ \AA}^{-1}$ . However, between  $k_{\parallel} = 0.13 \text{ \AA}^{-1}$  and  $k_{\parallel} = 0.16 \text{ \AA}^{-1}$ , the NCD signal decreases, changes its sign, and raises towards higher negative values with increasing parallel momentum  $k_{\parallel}$ . Also, the magnitude of the highest dichroism signal is more than four times larger than the maximum value before the change of sign. The highest value is reached at the point where the quantum-well band changes its dispersion. This behavior matches the expected behavior of the  $k_{\parallel}$ -dependent OAM signal as illustrated in Fig. 2(a), red dashed line, for the intermediate SOC case. Also, considering the dependence of SOC on the atomic number  $Z^4$ , the Pb/Cu(111) system can clearly be placed between the extrema of small SOC as, for instance, Cu and Au, and large SOC, as the topological insulator  $\text{Bi}_2\text{Se}_3$ . Hence, our measurements so far confirm the theoretically proposed OAM behavior by Kim *et al.*<sup>6</sup>

Nevertheless, there are currently various other proposed models to explain CD-ARPES signal.<sup>23–26</sup> For example,

Scholz *et al.* recently showed that the circular dichroism strongly depends on the used photon energy and can therefore also be assigned to a final-state effect.<sup>24</sup> However, this model does not seem to be capable of explaining the change of CD signal at finite momentum observed here. Another possibility to induce our observed behavior might be a strong band warping effect,<sup>27</sup> which we first need to exclude for our system before further conclusions can be made.

### 3. Out-of-plane orbital angular momentum

For the surface state of the topological insulator Bi<sub>2</sub>Te<sub>3</sub>, Jung *et al.*<sup>27</sup> found an energy dependence of the circular dichroism signal, which is an indication for an out-of-plane spin polarization component,<sup>28,29</sup> and which also could lead to the above observed  $k_{\parallel}$  dependence of the NCD signal. In order to exclude such a possible band warping effect for our Pb/Cu(111) system, we therefore measure now the out-of-plane OAM components with the experimental geometry shown in Fig. 1(b). The results are shown in Figs. 5(c) and 5(d). Again, in Fig. 5(c) the 2PPE spectra for right and left circularly polarized light and the resulting NCD signal are shown. As one can see from the dichroism spectra, almost no NCD is observable. To get a closer look, we again extracted the dichroism values along the quantum-well band and plotted the values as a function of emission angle respectively parallel momentum  $k_{\parallel}$  [see Fig. 5(d)]. Within the whole band, the absolute values stay below 4% and do not increase with increasing parallel momentum  $k_{\parallel}$  as was the case for the in-plane component. In contrast, if the system would exhibit

a relevant out-of-plane component of the OAM vector, it should also increase for increasing  $k_{\parallel}$ . However, we observe only small dichroism signals, which can be attributed to the purely geometric effect, as has been discussed for low symmetric setups by Jung *et al.*<sup>27</sup> Therefore, we can certainly exclude a strong band warping effect as the reason for the observed behavior of the NCD signal discussed above. As no out-of-plane component can be found, the circular dichroism in the Pb/Cu(111) quantum-well system can be explained by sensitivity of CD-ARPES to OAM texture, as proposed by Kim *et al.*<sup>6</sup>

## IV. CONCLUSION

In conclusion, 1 ML Pb/Cu(111) presents a Rashba system with intermediate SOC strength, where the OAM vector of the inner band is proposed to change its direction pointing antiparallel to the OAM vector of the outer band for small  $k_{\parallel}$  values, and parallel to the OAM vector of the outer band for larger  $k_{\parallel}$  values.<sup>6</sup> In consequence, the circular dichroism signal for the inner band should change its sign at finite  $k_{\parallel}$  in our experimental geometry, and we see such a predicted behavior in our measurements. We therefore support the idea of local OAM in Rashba-type spin-orbit split systems as proposed by Kim *et al.*<sup>6</sup> Furthermore, our results confirm the sensitivity of CD-ARPES to OAM texture in addition to spin.<sup>16</sup>

## ACKNOWLEDGMENT

S.J. is a recipient of a fellowship through the Excellence Initiative (DFG/GSC 266).

\*jakobs@physik.uni-kl.de

<sup>1</sup>Y. A. Bychkov and É. I. Rashba, Pis'ma Zh. Eksp. Teor. Fiz. **39**, 66 (1984).

<sup>2</sup>M. Hoesch, M. Muntwiler, V. N. Petrov, M. Hengsberger, L. Patthey, M. Shi, M. Falub, T. Greber, and J. Osterwalder, *Phys. Rev. B* **69**, 241401 (2004).

<sup>3</sup>J. H. Dil, F. Meier, J. Lobo-Checa, L. Patthey, G. Bihlmayer, and J. Osterwalder, *Phys. Rev. Lett.* **101**, 266802 (2008).

<sup>4</sup>F. Meier, H. Dil, J. Lobo-Checa, L. Patthey, and J. Osterwalder, *Phys. Rev. B* **77**, 165431 (2008).

<sup>5</sup>S. Mathias, A. Ruffing, F. Deicke, M. Wiesenmayer, I. Sakar, G. Bihlmayer, E. V. Chulkov, Y. M. Koroteev, P. M. Echenique, M. Bauer *et al.*, *Phys. Rev. Lett.* **104**, 066802 (2010).

<sup>6</sup>B. Kim, C. Kim, P. Kim, W. Jung, Y. Kim, Y. Koh, M. Arita, K. Shimada, H. Namatame, M. Taniguchi *et al.*, *Phys. Rev. B* **85**, 195402 (2012).

<sup>7</sup>C. R. Ast, J. Henk, A. Ernst, L. Moreschini, M. C. Falub, D. Pacilé, P. Bruno, K. Kern, and M. Grioni, *Phys. Rev. Lett.* **98**, 186807 (2007).

<sup>8</sup>J. Premper, M. Trautmann, J. Henk, and P. Bruno, *Phys. Rev. B* **76**, 073310 (2007).

<sup>9</sup>H. Mirhosseini, J. Henk, A. Ernst, S. Ostanin, C.-T. Chiang, P. Yu, A. Winkelmann, and J. Kirschner, *Phys. Rev. B* **79**, 245428 (2009).

<sup>10</sup>L. Moreschini, A. Bendounan, I. Gierz, C. Ast, H. Mirhosseini, H. Höchst, K. Kern, J. Henk, A. Ernst, S. Ostanin *et al.*, *Phys. Rev. B* **79**, 075424 (2009).

<sup>11</sup>S. R. Park, C. H. Kim, J. Yu, J. H. Han, and C. Kim, *Phys. Rev. Lett.* **107**, 156803 (2011).

<sup>12</sup>J.-H. Park, C. H. Kim, J.-W. Rhim, and J. H. Han, *Phys. Rev. B* **85**, 195401 (2012).

<sup>13</sup>Y. Ohtsubo, J. Mauchain, J. Faure, E. Papalazarou, M. Marsi, P. Le Fèvre, F. Bertran, A. Taleb-Ibrahimi, and L. Perfetti, *Phys. Rev. Lett.* **109**, 226404 (2012).

<sup>14</sup>H. Lee and H. J. Choi, *Phys. Rev. B* **86**, 045437 (2012).

<sup>15</sup>S. Park, J. Han, C. Kim, Y. Koh, C. Kim, H. Lee, H. Choi, J. Han, K. Lee, N. Hur *et al.*, *Phys. Rev. Lett.* **108**, 046805 (2012).

<sup>16</sup>Y. H. Wang, D. Hsieh, D. Pilon, L. Fu, D. R. Gardner, Y. S. Lee, and N. Gedik, *Phys. Rev. Lett.* **107**, 207602 (2011).

<sup>17</sup>J. Henrion and G. Rhead, *Surf. Sci.* **29**, 20 (1972).

<sup>18</sup>S. Müller, J. E. Prieto, C. Rath, L. Hammer, R. Miranda, and K. Heinz, *J. Phys.: Condens. Matter* **13**, 1793 (2001).

<sup>19</sup>S. Mathias, A. Ruffing, F. Deicke, M. Wiesenmayer, M. Aeschlimann, and M. Bauer, *Phys. Rev. B* **81**, 155429 (2010).

<sup>20</sup>J. H. Dil, *J. Phys.: Condens. Matter* **21**, 403001 (2009).

<sup>21</sup>Note that defining OAM to be positive or negative is just convention, but essential to easily describe the results.

<sup>22</sup>The spectra from individual measurements were stitched together to get an overview of the full-angle distribution photoemission maps. Therefore, all physical quantities shown in our paper are extracted from the original data sets.

- <sup>23</sup>H. Zhang, C.-X. Liu, and S.-C. Zhang, arXiv:[1211.0762v1](#).
- <sup>24</sup>M. R. Scholz, J. Sánchez-Barriga, J. Braun, D. Marchenko, A. Varykhalov, M. Lindroos, Y. J. Wang, H. Lin, A. Bansil, J. Minár *et al.*, [Phys. Rev. Lett. \*\*110\*\*, 216801 \(2013\)](#).
- <sup>25</sup>C. Jozwiak, C.-H. Park, K. Gotlieb, C. Hwang, D.-H. Lee, S. G. Louie, J. D. Denlinger, C. R. Rotundu, R. J. Birgeneau, Z. Hussain *et al.*, [Nat. Phys. \*\*9\*\*, 293 \(2013\)](#).
- <sup>26</sup>Y. Cao, J. A. Waugh, X.-W. Zhang, J.-W. Luo, Q. Wang, T. J. Reber, S. K. Mo, Z. Xu, A. Yang, J. Schneeloch, G. Gu, M. Brahlek, N. Bansal, S. Oh, A. Zunger, and D. S. Dessau, arXiv:[1209.1016v1](#).
- <sup>27</sup>W. Jung, Y. Kim, B. Kim, Y. Koh, C. Kim, M. Matsunami, S.-i. Kimura, M. Arita, K. Shimada, J. H. Han *et al.*, [Phys. Rev. B \*\*84\*\*, 245435 \(2011\)](#).
- <sup>28</sup>L. Fu, [Phys. Rev. Lett. \*\*103\*\*, 266801 \(2009\)](#).
- <sup>29</sup>S. Basak, H. Lin, L. A. Wray, S.-Y. Xu, L. Fu, M. Z. Hasan, and A. Bansil, [Phys. Rev. B \*\*84\*\*, 121401 \(2011\)](#).